

Article

Optimized Route Planning under the Effect of Hull and Propeller Fouling and Considering Ocean Currents

Ageliki Kytariolou and Nikos Themelis * 

School of Naval Architecture and Marine Engineering, National Technical University of Athens, 15780 Athens, Greece; akytariolou@deslab.ntua.gr

* Correspondence: nthemelis@naval.ntua.gr

Abstract: Route planning procedures for ocean-going vessels depend significantly on prevailing weather conditions, the ship's design characteristics and the current operational state of the vessel. The operational status considers hull and propeller fouling, which significantly affects fuel oil consumption coupled with route selection. The current paper examines the effect of the fouling level on the selection of the optimized route compared with the clean hull/propeller as well as the orthodrome/loxodrome route. A developed weather routing tool is utilized, which is based on a physics-based model for the calculation of the main engine's fuel oil consumption enriched to account for different fouling levels of the hull and the propeller. A genetic algorithm is employed to solve the optimization problem. A case regarding a containership in trans-Atlantic transit using forecasted weather data is presented. The effect of ocean currents is also examined as it was derived that they greatly affect route selection, revealing a strong dependence on the level of fouling. Ignoring the fouling impact can result in miscalculations regarding the estimated fuel oil consumption for a transit. Similarly, when ocean currents are ignored in the route planning process, the resulting optimal paths do not ensure energy saving.

Keywords: weather routing; ocean currents; fouling; fuel oil consumption; route optimization



Citation: Kytariolou, A.; Themelis, N. Optimized Route Planning under the Effect of Hull and Propeller Fouling and Considering Ocean Currents. *J. Mar. Sci. Eng.* **2023**, *11*, 828. <https://doi.org/10.3390/jmse11040828>

Academic Editor: Tie Li

Received: 23 February 2023

Revised: 5 April 2023

Accepted: 11 April 2023

Published: 13 April 2023



Copyright: © 2023 by the authors. Licensee MDPI, Basel, Switzerland. This article is an open access article distributed under the terms and conditions of the Creative Commons Attribution (CC BY) license (<https://creativecommons.org/licenses/by/4.0/>).

1. Introduction

In recent years, ship energy efficiency and greener operation have been highlighted as areas in need of improvement in the marine industry. As a result of increasing pressure, environmental concern has become among the major priorities in the industry, even though marine trade is already known to be the most efficient means of transportation in terms of emissions per ton of cargo. The International Maritime Organization (IMO) has introduced a stricter regulatory framework for reducing ship emissions [1]. Improvements can be made not only in terms of design optimization but also via more efficient and optimized operation [2], targeting the reduction in fuel oil consumption and, consequently, greenhouse gas emissions. Fuel oil consumption depends mainly on the total resistance that a ship faces during the journey. Route planning aims to save a significant amount of fuel via route optimization techniques, especially when the prevailing weather conditions of the voyage are considered. Calm water resistance is usually the dominant resistance for cargo ships operating at moderate speeds. This component's value increased over time due to the increase in frictional drag. This is a result of hull and propeller fouling, which occurs as the ship operates or even when moored. The roughness of the surface of the hull and the propeller increases due to fouling, when micro- and macro-organisms accumulate on the surface of the vessel. Fouling of the hull and/or the propeller can lead to increased frictional drag, and antifouling coatings and proper cleaning actions in dry docking can save fuel.

This paper focuses on the impacts of hull and propeller fouling status on the problem of optimal route selection. The effect of ocean currents within the optimization process

has also been considered, as the impact of ocean currents is significant especially when the fouling level is high. In Section 2, a brief literature review is presented, highlighting works that have examined the connection between fouling effects and fuel oil consumption. Moreover, since reducing fuel oil consumption is the main objective function for route optimization problems, works concerning weather routing are also discussed, along with studies that integrate the effect of ocean currents in the route planning procedure. In Section 3, a brief description of the developed weather routing tool is presented. The tool is characterized by a physics-based model for the calculation of the main engine fuel oil consumption, which is presented in Section 4. The incorporation of hull and propeller fouling impacts on the physics-based model is presented in Section 5. Finally, in Section 6, a study about optimal route selection for a containership is presented using different levels of hull and/or propeller fouling. A key aim of this study is the comparison between fuel oil consumption for the optimal path found with clean conditions and the respective consumption for the fouled cases examined for this fixed path. Moreover, the impact of sea currents on optimized route selection is additionally examined. Section 7 contains the conclusions of the present work related to the impact of fouling and ocean currents within the route optimization process.

2. Literature Review

It is well known that ship operations and even mooring conditions deteriorate hull and propeller fouling statuses over time. The roughness of the hull and propeller can lead to a significant increase in power demands for the main engine, resulting not only in increased fuel oil consumption but also in unsafe operations in heavy sea conditions. In [3], the effect of hull roughness on the ship's performance is presented both in calm water and in real sea conditions. Assuming different levels of hull fouling, results show that calm water resistance can be affected over years of operation due to fouling, leading to increased brake power (12%) and fuel oil consumption (21%). Additionally, the combined effect of fouling and the added wave resistance in high sea states can result in power demands that exceed the limits of the main engine. Liu et al. in [4] concluded that it is possible that ships fulfilling the IMO [5] requirements for minimum propulsion power in adverse weather conditions may not satisfy these requirements when fouling is taken into account. The influence of propeller and/or hull roughness was investigated, noting the actual condition of a ship in service and the impact of the roughness of the hull and the propeller separately since the two surfaces deteriorate at different rates. Similarly, Schultz [6] presented a prediction method to estimate the increase in resistance and power due to fouling for a full-scale ship based on model-scale tests and layer similarity law analyses. A benchmark frigate was used for the calculations, showing that power demands can increase by up to 86% for heavy fouling conditions and a service speed equal to 15 knots; for the same hull conditions but double the service speed, power demands can increase by approximately 60%, indicating that residual resistance becomes dominant at higher speeds and is less affected by fouling.

The loading condition, ship speed, and heading are among the parameters that influence fuel oil consumption during transit. Optimal route selection is therefore a process that combines all these parameters under certain constraints with the aim to lower fuel costs and emissions. In [7], a method to predict voyage duration and CO₂ emissions was proposed while considering safety and environmental aspects. Speed loss is taken into consideration, pointing out its influence on fuel oil consumption. In Kytariolou and Themelis [8], a new weather routing tool was presented. The tool aimed to calculate the optimal path, in terms of fuel oil consumption, while considering weather forecast data and predefined safety criteria. It is well known that environmental factors affect fuel oil consumption and the safety of the voyage. In [9], the three-dimensional modified isochrone (3DMI) method was applied to solve the ship routing problem considering environmental elements such as wind, wave, and ocean currents. Optimization was performed following two different strategies—estimated time of arrival (ETA routing) and minimum fuel oil consumption

(FUEL routing)—along with different constraints. Results show that when aiming to reduce fuel oil consumption, the optimal path requires more time and distance to be travelled in comparison with ETA routing. In addition, when safety constraints are also considered in the optimization process, for both cases, total fuel oil consumption and voyage duration are negatively impacted. Kurosawa et al. [10] developed a new routing system based on the A* algorithm, targeting coastal seas. The optimization considered the shortest distance, the minimum travelling time, and the minimum fuel oil consumption. Atmospheric and oceanic data were considered—whenever the data were updated, the optimal trajectory was recalculated. In addition, Shin et al. [11] proposed an improved A* algorithm to find the optimal path for economical ship operations. The improved method was based on an adaptive grid system, reducing exhaustive calculations required by the original A* algorithm. The validity of the new method was highlighted via a presented case study, where the original and improved methods were both utilized.

Vettor and Soares [12] present a routing code, aiming at the minimization of fuel oil consumption under exposure to severe seas. Strip theory is used for hydrodynamic calculations (RAOs and added wave resistance), while the method of Holtrop and Mennen was used for the calm water resistance estimation. With all this information available, the code derives an optimal route that bypasses dangerous sea areas, which would also affect fuel oil consumption. Ocean currents also play an important role in route selection. Transit time and fuel oil consumption are significantly affected by current flow; therefore, when their impact is taken into account, ship route planning can be improved. Chang et al. [13] and Chen and Sasa [14] emphasize utilizing the strong ocean current of Kuroshio in the North Pacific. When avoiding sailing against the current, it is mentioned that time and fuel can be saved even when sailing greater distances than the orthodromic path. In addition, in Yang et al. [15], the importance of currents in speed optimization is highlighted. The proposed method takes into consideration the effect of currents by utilizing a speed correction model that can distinguish speed through water (STW) from speed over ground (SOG). Thus, by using the corrected speed, results concerning ETA and fuel oil consumption are more accurate. The presented case study showed that the estimated and measured SOG for a real voyage of a tanker when currents are accounted for can be reduced by more than 3%. Similarly, in Mannarini et al. [16], a model of ship routing named VISIR is presented, highlighting the impact of sea currents in route selection. Even in the presence of waves, when sea currents are taken into consideration, route duration and topology can differ significantly compared to route planning that ignores current flows completely.

Li and Zhang [17] examined the relationship between minimum fuel oil consumption and the ship's motion control system. They propose a robust energy-saving algorithm to control course keeping and a ship's motions. The designed controller employs a third-order closed-loop gain-shaping algorithm, while the nonlinear switching feedback technique is used for the final control law. Simulations are presented under normal and heavy sea conditions, while results are compared with a nonlinear decoration controller. Results show that the accuracy of course keeping improves and yaw is reduced, while settling and delay times are shortened; thus, the energy consumption of the steering gear is positively affected.

The topics of course-keeping control and path following play more crucial roles in unmanned vessels (e.g., [18,19]). In Zhang et al. [20], the tracking problem of an autonomous surface vehicle (ASV) is solved by using a robust controller. The trajectory-tracking method presented employs a neural network, while uncertainty dynamics and unavailable velocity are present. Similarly, Qin and Du [21] present a finite-time event-triggered control system for unmanned surface vehicles (USVs). The presented trajectory tracking issue is addressed, while the effects of input saturation, parametric uncertainties, and unstable environments are considered concurrently.

3. Weather Routing Tool

The weather routing tool used in the current study is developed in the MATLAB environment [8], and Figure 1 presents the respective calculation framework. The tool

can generate random routes between a port of departure to a given port of arrival. For each one of these routes, fuel oil consumption can be calculated by considering the ship’s characteristics and prevailing weather conditions. A physics-based model for the calculation of the main engine fuel oil consumption required to sail from a specific point of the route to the next one has been developed. The main engine and propeller model estimates the required power needed to sustain a requested ship speed. For these calculations, the ship’s total resistance is calculated, entailing calm water, added wave, and wind resistance components. The developed tool allows each one of these components to be evaluated by employing models of different fidelity levels (e.g., CFD and empirical formulas). For the current study, calm water resistance is calculated using the Holtrop–Mennen method [22], wave-added resistance is calculated using a 3D panel code named NEWDRIFT+ [23,24], and wind resistance is calculated by using Blendermann’s coefficients [25].

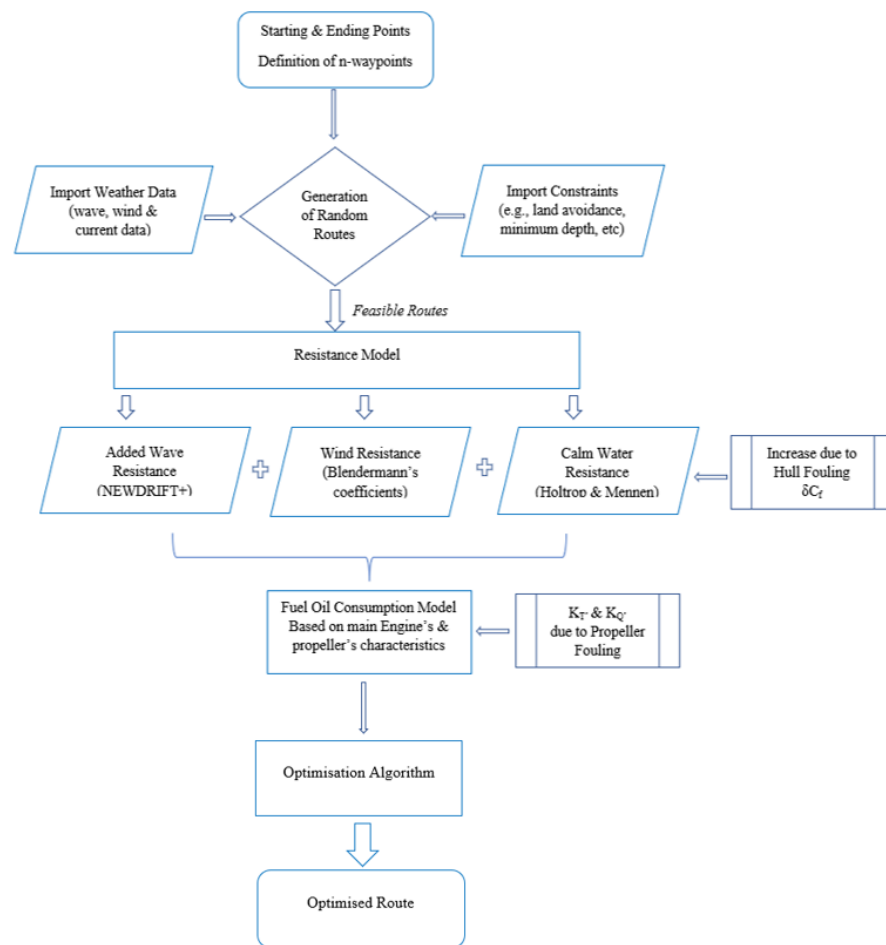


Figure 1. Flowchart of the presented weather routing tool.

The calm water resistance calculation is performed initially by assuming the hull and the propeller are fully cleaned. However, this condition changes continuously during the ship’s operation and degrades further when the ship remains in ports. As mentioned previously, the accumulation of the organisms on hull and propeller surfaces results in their roughness. This phenomenon leads to the deterioration of coatings (e.g., corrosion) and an increase in drag resistance, which consequently increase fuel oil consumption. The degree of roughness concerning the hull and the propeller is different, and for this reason, an individual coefficient is used to represent the roughness of each surface. The effect of hull fouling will be considered via an increase in the calm water resistance by modifying the frictional resistance coefficient, while propeller fouling is considered by modifying its open water characteristics.

4. Calculation of the Main Engine’s Fuel Oil Consumption

According to Equation (1), the ship’s total resistance (R_{tot}) is calculated as follows:

$$R_{tot} = R_{calm} + R_{wave} + R_{wind} \tag{1}$$

where R_{calm} , R_{wave} , and R_{wind} refer to calm water, added wave and wind components of the resistance, respectively. Having determined the ship’s total resistance, the brake power can be calculated as follows:

$$P_B = R_{tot}V_S / (k\eta_S\eta_0\eta_H\eta_R) \tag{2}$$

where V_S is the ship’s speed; k corresponds to the number of the propellers; η_S is the shaft efficiency; η_0 is the propeller’s open water efficiency, which equals $(K_T J) / (K_Q 2\pi)$; η_H is the hull efficiency, which equals $(1 - t) / (1 - w)$; J is the advance coefficient; t is the trust deduction coefficient; and w is the wake coefficient, while η_R is the propeller’s total rotational coefficient.

When the propeller’s characteristics (diameter, pitch ratio, number of blades, and the ratio of the expanded blade area) are known and thrust and torque coefficient curves are provided, the quantities of K_T , K_Q , J , and n are determined using the propeller’s open water diagram, which corresponds to calm water conditions. Firstly, the following quantity is calculated:

$$K_T / J^2 = [T / (\rho n^2 D^4)] / (V / nD)^2 = T / (\rho V^2 D^2) = CC \tag{3}$$

where ρ is the water density, n is the propeller’s revolutions, D is the propeller’s diameter, and T is the thrust. From the intersection of curve $K_T = CCJ^2$ with the curve $(K_T - J)$ of the open water diagram of the propeller, the values of J , K_T , K_Q , and η_0 can be determined. Then, we have the following:

$$n = V_{ad} / (JD) \tag{4}$$

where $V_{ad} = V_S(1 - w)$ is the advance speed of the propeller when operating in the ship’s wake, and V_S is the ship’s speed.

Based on the main engine manufacturer’s manual and the information above, the specific fuel oil consumption (SFOC) can be calculated for any pair of $(n - P_B)$ using Equations (2) and (4). Then, between every two points of interest (named x_i and x_{i+1}), the corresponding fuel oil consumption (FOC_i) can be derived:

$$FOC_i = t_i SFOC(n_i, P_{Bi}) P_{Bi} \tag{5}$$

where t_i is the sailing time from x_i to x_{i+1} while assuming constant weather conditions and ship speed.

5. Fouling Impact

As already mentioned, the assumption of having a fully cleaned hull and propeller is a non-realistic scenario. To consider a realistic hull and propeller fouling performance status, the following method has been considered.

According to the ITTC [26], the roughness of the hull leads to an increase in the frictional resistance coefficient, as shown in Equation (6):

$$\delta C_f = 0.044[(k_S / L_{WL})^3 - 10Re^{(-1/3)}] + 0.000125 \tag{6}$$

where k_S is the equivalent sand roughness height of the hull surface, L_{WL} is the ship’s length at the waterline, Re is Reynolds number, and δC_f is the empirical roughness allowance.

Thus, the increased resistance due to hull fouling is calculated according to Equation (7):

$$R_{FL} = 1/2\rho S V_S^2 \delta C_f \tag{7}$$

where ρ is sea water density, S is the wetted surface of the hull, and V_S is the ship's speed. The quantity of R_{calm} in Equation (1) is now replaced with Equation (8).

$$R_{\text{calm_fouled}} = R_{\text{calm}} + R_{\text{FL}} \tag{8}$$

In addition, according to the ITTC [26] procedure, the increase in the roughness of the propeller surface on the open water characteristics is considered as follows:

$$K_{\text{TS}} = K_{\text{TM}} - \Delta K_{\text{T}} \tag{9}$$

$$K_{\text{QS}} = K_{\text{QM}} - \Delta K_{\text{Q}} \tag{10}$$

where K_{TS} and K_{QS} are the thrust and torque coefficients of the full-scale propeller incorporating the fouling impact; K_{TM} and K_{QM} are the thrust and torque coefficients without fouling, while according to [18]; and ΔK_{T} and ΔK_{Q} are derived by Equations (11) and (12), respectively:

$$\Delta K_{\text{T}} = -0.3\Delta C_{\text{D}}(p/D)(c/D)Z \tag{11}$$

$$\Delta K_{\text{Q}} = 0.25\Delta C_{\text{D}}(c/D)Z \tag{12}$$

where ΔC_{D} is the difference in the drag coefficient:

$$\Delta C_{\text{D}} = C_{\text{DM}} - C_{\text{DS}} \tag{13}$$

and

$$C_{\text{DM}} = 2(1 + 2.0t_{\text{p}}/c)[0.044/(Re_{\text{co}})^{1/6} - 5/(Re_{\text{co}})^{2/3}] \tag{14}$$

$$C_{\text{DS}} = 2(1 + 2.0t_{\text{p}}/c)[1.89 + 1.62\log(c/k_{\text{p}})]^{-2.5} \tag{15}$$

In Equations (14) and (15), c is the chord length at $x = 0.75R$, R is the propeller radius, t_{p} is the maximum thickness, Z is the number of blades, p/D is the pitch ratio, Re_{co} is the Reynolds number at $x = 0.75R$ in the open water test based on the chord length and local velocity, and k_{p} is the roughness of the propeller blade, which reflects the propeller's fouling.

6. Case Study

6.1. Examined Ship, Route, and Fouling Cases

For demonstration purposes, the selected ship is a containership, for which its basic characteristics are shown in Table 1, while the propeller's characteristics needed for the calculations are shown in Table 2. The chosen route is between Europe and North America. The port of departure is the port of Lisbon (Portugal), whereas the port of arrival is the port of Halifax (Canada, Nova Scotia). In Figure 2 the corresponding orthodrome path between the ports of departure and arrival is shown. Optimization has been performed for several cases representing different hull and propeller fouling conditions, described below as cases 1 to 5. In addition, the ship's speed, and specifically the commanded SOG, is assumed to be constant and equal to 18 kn:

- Case 1: Clean hull and propeller;
- Case 2: Hull fouling represented with $k_{\text{s}} = 5000 \mu\text{m}$ (mentioned as medium hull fouling) and clean propeller;
- Case 3: Hull fouling represented with $k_{\text{s}} = 10,000 \mu\text{m}$ (mentioned as heavy hull fouling) and clean propeller;
- Case 4: Hull fouling represented with $k_{\text{s}} = 5000 \mu\text{m}$ and propeller fouling represented with $k_{\text{p}} = 1000 \mu\text{m}$ (mentioned as medium hull and propeller fouling);
- Case 5: Hull fouling represented with $k_{\text{s}} = 10,000 \mu\text{m}$ and propeller fouling represented with $k_{\text{p}} = 2000 \mu\text{m}$ (mentioned as heavy hull and propeller fouling).

Table 1. Containership’s characteristics.

Parameter	Value
Length B.P. (m)	244.80
Breadth (m)	32.25
Depth (m)	19.30
Draft Sc. (m)	12.60
TEU	4250
DWT (t)	50,829
Main Engine (kW)	37,046.4
Service Speed (m)	24.5

Table 2. Propeller’s characteristics.

Parameter	Value
Chord–Diameter ratio at $0.7R$	0.3019
Thickness–Diameter ratio at $0.7R$	0.0144
Number of Blades Z	6
Diameter of ship propeller D (m)	7.8
Mean Pitch–Diameter ratio p/D	0.975
Propeller Revolutions n_{prop} (rps)	12

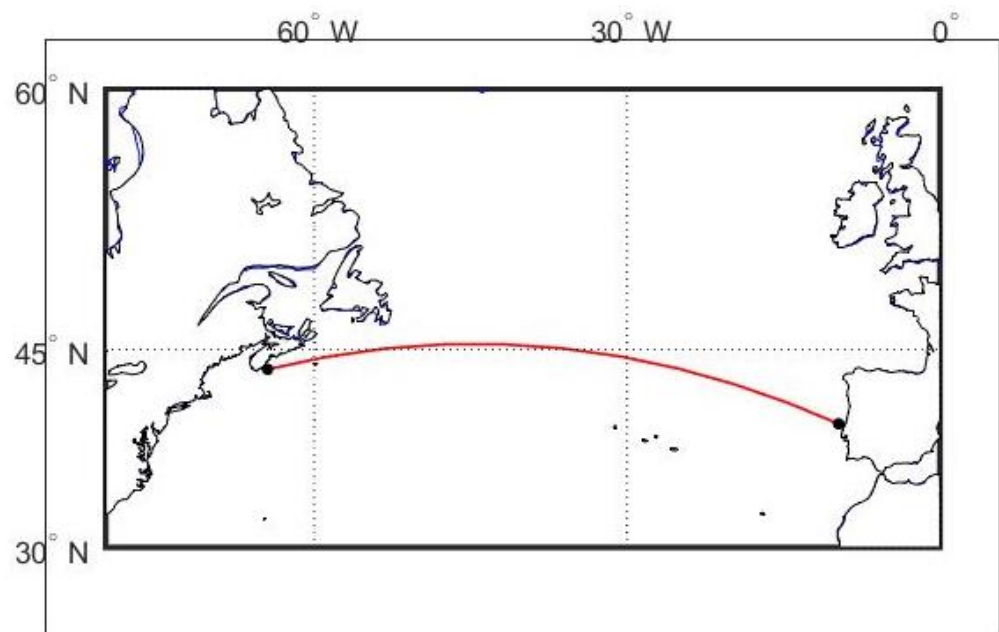


Figure 2. Orthodrome path for the chosen route between Europe and North America.

6.2. Fouling Impact

In Figure 3, the effect of the propeller’s fouling on the propeller’s characteristic curves is shown for Case 4 and Case 5 ($k_p = 1000 \mu\text{m}$ and $k_p = 2000 \mu\text{m}$, respectively) compared with the respective curves corresponding to the clean condition of the propeller.

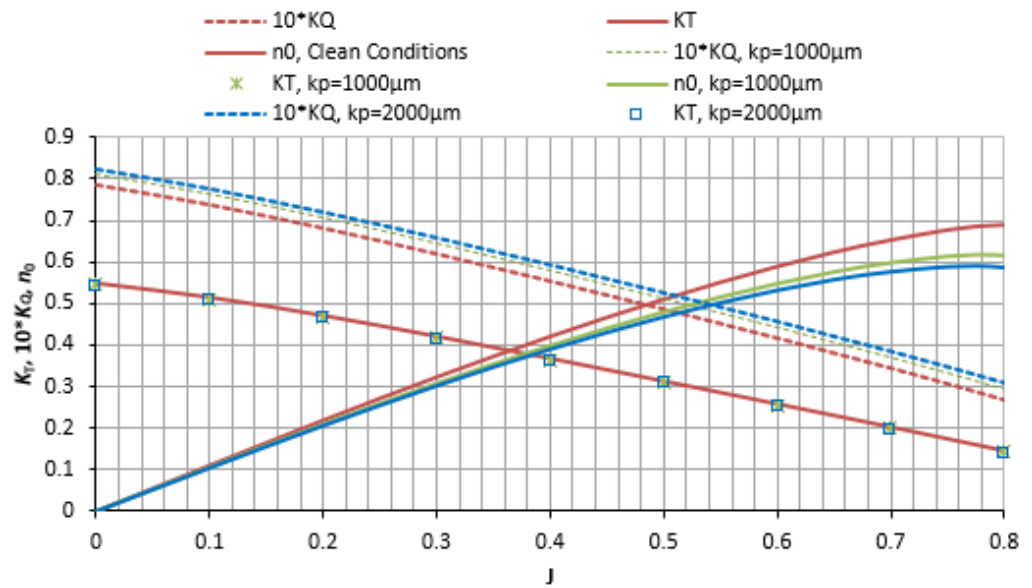


Figure 3. Propeller’s fouling effect on propeller’s open water characteristic curves.

It has already been mentioned that hull fouling acts on calm water resistance negatively (Figure 4). Calm water resistance in medium fouling conditions increases by about 25% compared with clean hull conditions, while a more than 50% increase is observed in heavy fouling condition.

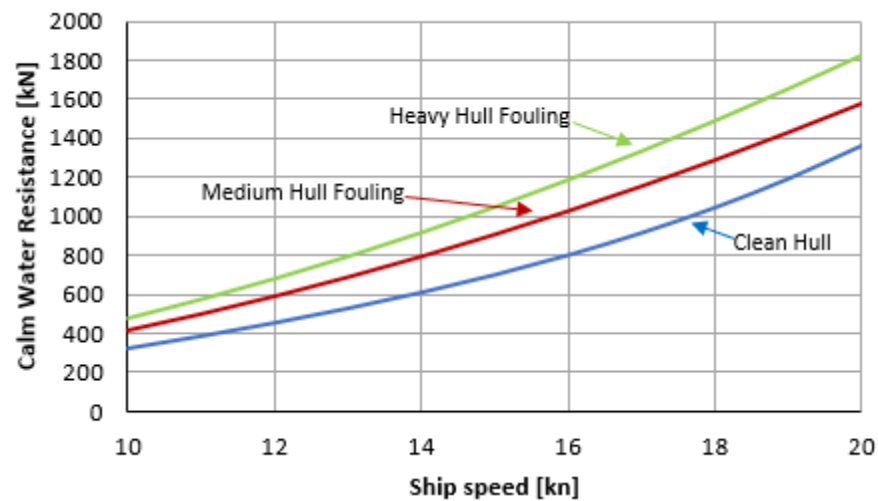


Figure 4. Impact of fouling on calm water resistance curves.

In addition, the impact of sea currents has been considered by correcting the speed value (STW) for calm water resistance calculations as follows:

- STW minus the currents’ velocity when the currents’ flow direction is the same as the ship’s direction.
- STW plus the currents’ velocity when the currents’ flow direction is the opposite of the ship’s direction.

6.3. Optimisation Set Up

For all cases, the journey starts on 23 February 2019 at 21.00, and optimization is performed for four waypoints utilizing a genetic algorithm embedded in MATLAB [27] with one hundred generations and one hundred populations each. An example of the algorithm’s evolution that corresponds to the clean hull and propeller (Case 1) is shown in Figure 5,

where the red circle indicates the optimal route. Some routes were neglected from the process and characterized as unfeasible because they violate the land avoidance principle.

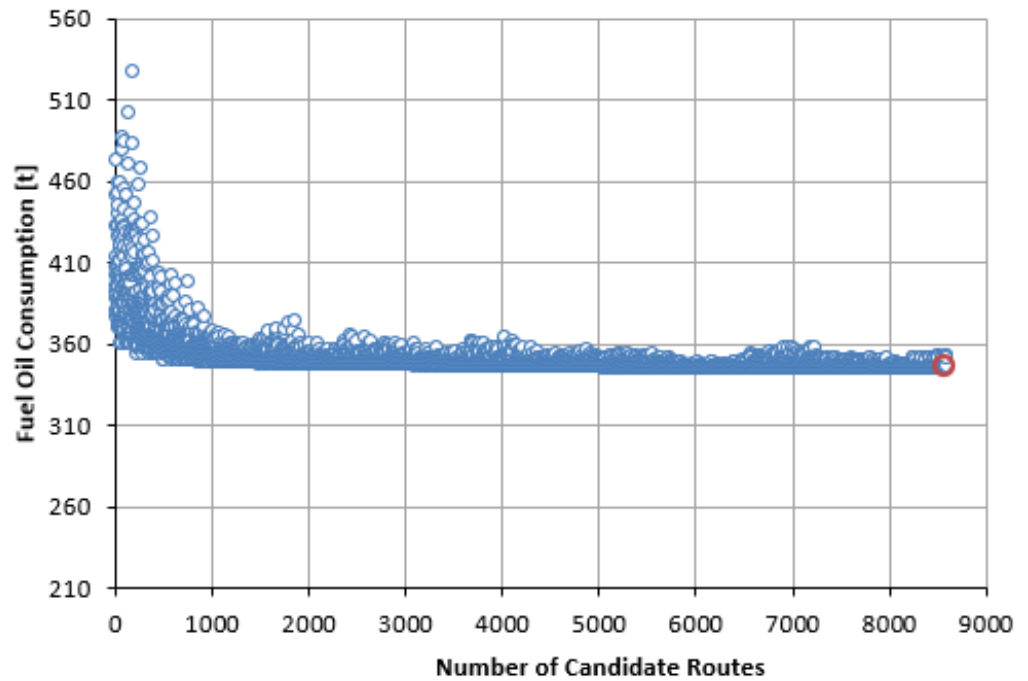


Figure 5. Algorithm’s evolution with constant speed and clean hull and propeller.

6.4. Examination of the Impact of Fouling on the Orthodromic Path

It is well expected that hull fouling will eventually lead to a frictional resistance increase and consequently to higher calm water resistance. This increase is shown in Figure 6, where the orthodromic route is examined for the voyage mentioned above for three different hull conditions.

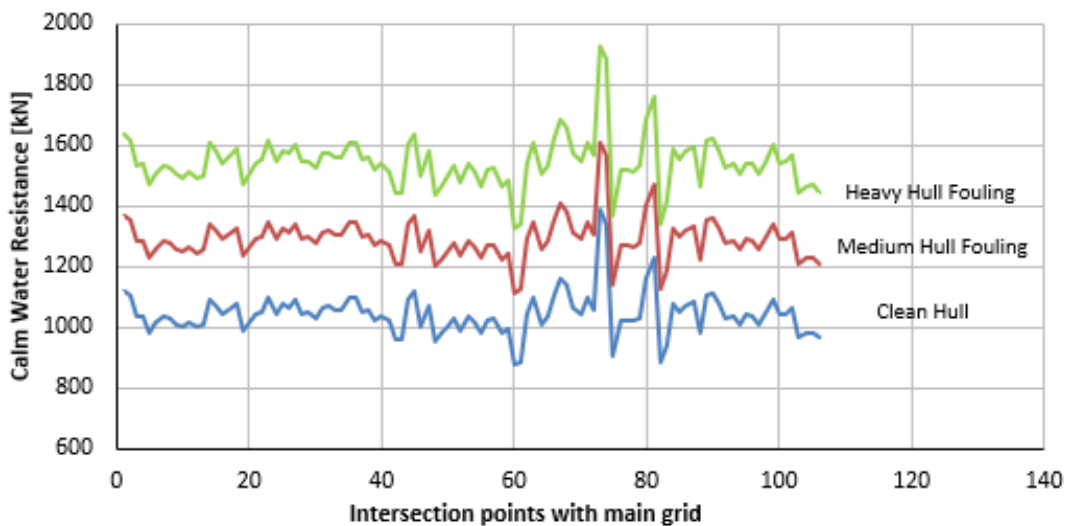


Figure 6. Calm water resistance increase due to fouling along the orthodrome path.

When the propeller’s fouling is added to the problem, fuel oil consumption (FOC) increased by 15% compared with the fouled hull with a clean propeller (Table 3).

Table 3. Comparison of orthodromic paths.

	Orthodrome				
	Clean Hull (Case 1)	Medium Hull Fouling (Case 2)	Heavy Hull Fouling (Case 3)	Medium Hull and Propeller Fouling (Case 4)	Heavy Hull and Propeller Fouling (Case 5)
FOC (t)	362.7	451.9 (+24.6%)	548.7 (+51.2%)	521.3 (+43.7%)	655.2 (+80.6%)
Voyage duration (h)	133.5				
Distance (nm)	2402.2				

6.5. Examination of the Impact of Hull and Propeller Fouling on Optimized Routes

The optimal paths found by the genetic algorithm for different statuses of the vessel are shown in Figure 7. An analysis of the encountered weather conditions in each optimized route, as well as the calculated resistance and fuel oil consumption in each case, is presented next. In Figure 8, the currents' velocity encountered by the ship along the optimal paths for each hull condition is presented. The negative values indicate the current flowing opposite the ship's direction. As hull fouling and, subsequently, demanded power increase, the algorithm seeks favorable paths in which calm water resistance is lowered as much as possible (Figure 9). This trend is much more noticeable when the heavy fouling condition is assumed. To save fuel, calm water resistance and wave-added resistance (Figure 10), the two main components of the total resistance, must be as low as possible along the route. However, the attempt to keep both components low may be a contradictory scenario. Therefore, a compromise should be made, and it is noticeable that as hull fouling increases, this compromise favors a decrease in calm water resistance since it affects the total resistance more than the added wave resistance component.

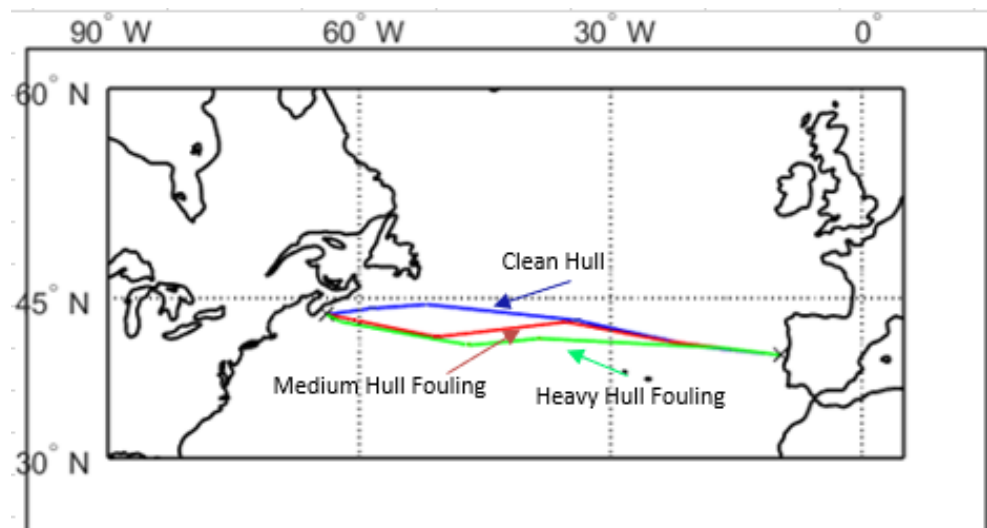


Figure 7. Optimal routes with a constant speed of 18 kn for Cases 1 (clean hull), 2 (medium hull fouling), and 3 (heavy hull fouling).

The points mentioned in the *x*-axis in the following figures correspond to the points that intersect with the main grid. Since the spatial resolution of the wave, wind, and current data may be different, the wave resolution is the chosen one to form the main grid, while information about wind and current on the main grid is obtained via linear interpolation [8].

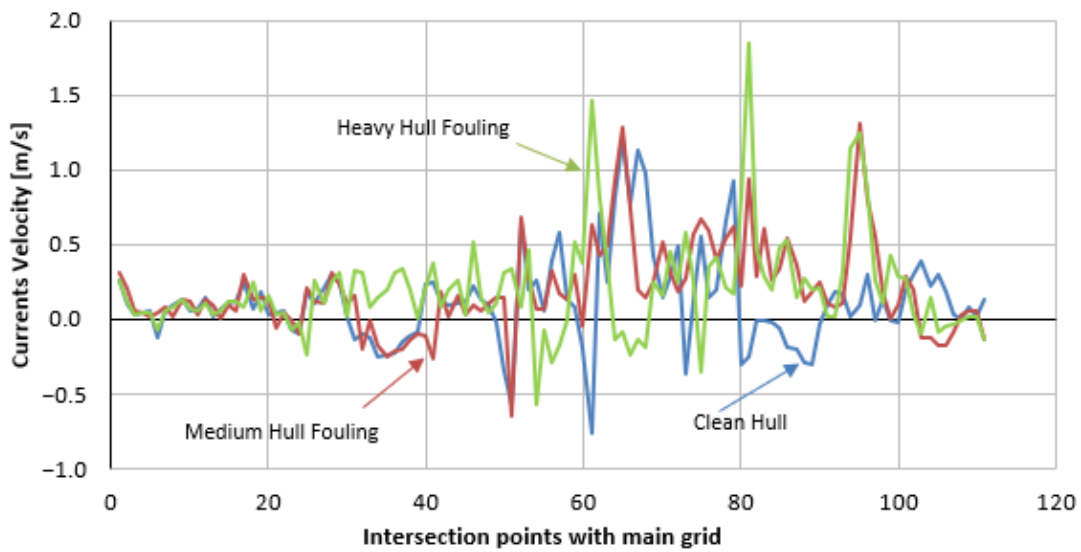


Figure 8. Currents' velocity along the optimal paths for different hull fouling conditions.

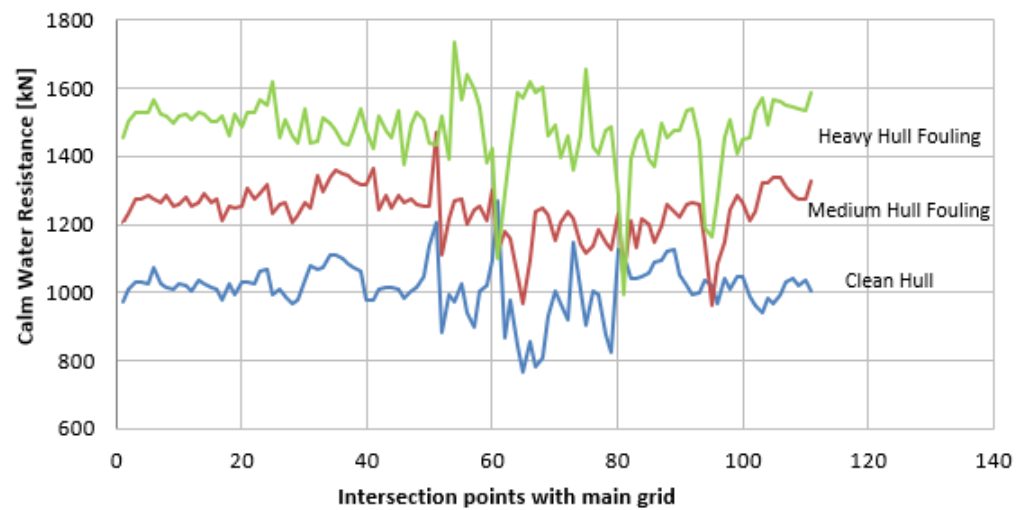


Figure 9. Calm water resistance corresponding to optimum paths for different hull fouling conditions.

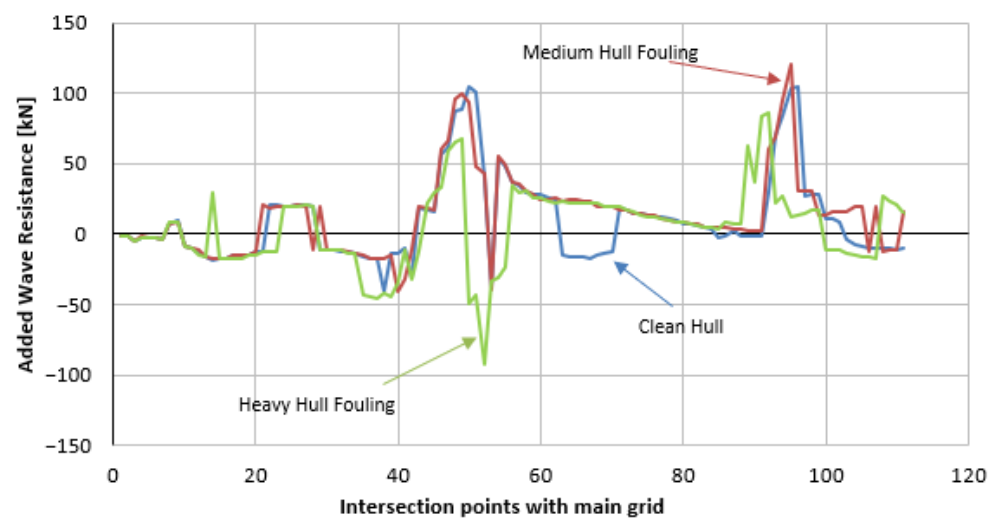


Figure 10. Added wave resistance corresponding to optimum paths for different hull fouling conditions.

In Figures 11 and 12 the significant wave height and the relative heading along the routes with clean, medium, and heavy fouled hull are shown along the corresponding optimal paths. Following seas are represented with 0 deg., whereas head seas are represented with 180 deg. While the algorithm seeks favorable current paths, especially in the heavy fouling condition, optimal path may pass through sea areas where the significant wave height is increased (around intersection point No. 50). Nevertheless, the corresponding relative wave direction refers to following or near followings seas, which results in negatively added wave resistance values. These negative values indicate that the added wave resistance component positively impacts the total resistance of the vessel.

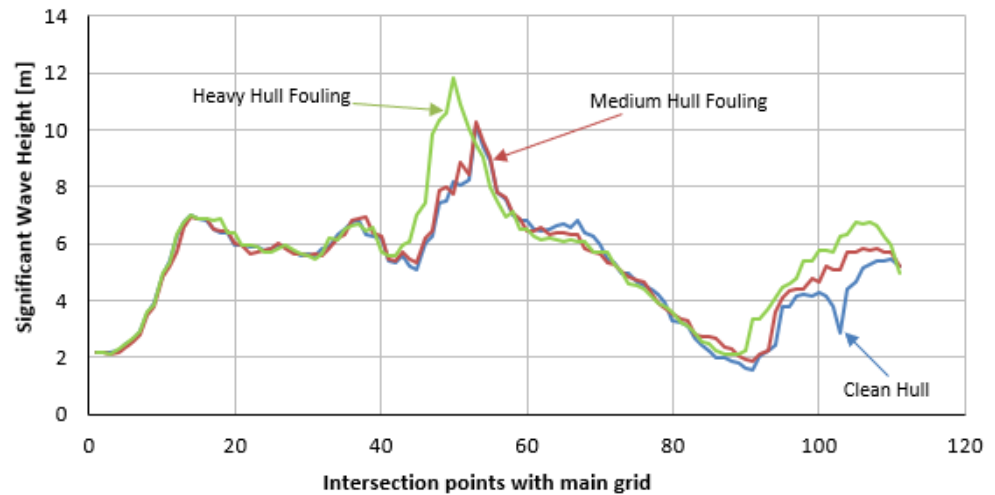


Figure 11. Prevailing significant wave height corresponding to optimum paths for different hull fouling conditions.

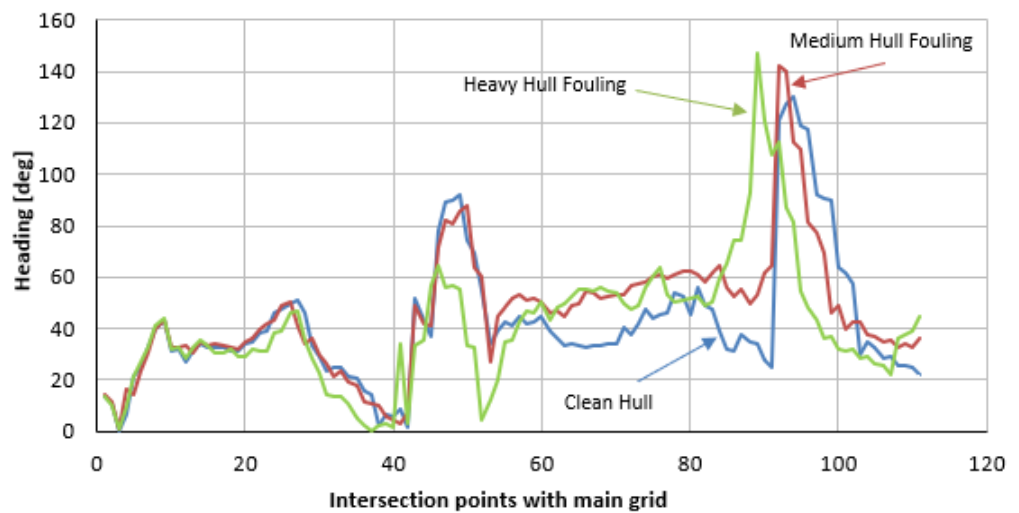


Figure 12. Relative wave heading corresponding to optimum paths for different hull fouling conditions.

It is interesting to examine the impact of not considering the fouling status of the hull and the propeller during the optimization process. As mentioned in the introduction, the idea here is to fix the identified optimal path for the clean hull and propeller condition (Case 1) and then derive the results for the other cases by utilizing this specific route.

Based on the results shown in Table 4, the gain from further optimization is minor. The optimal paths found with a fouled hull require about the same fuel oil consumption as the fixed optimal path of the clean hull when conducting the test described before. While the fouling level is higher, the algorithm seeks favorable current paths to prevent an increase

in calm water resistance. This forces the algorithm to follow paths with higher added wave and/or wind resistance while avoiding opposite current flows. These contradictory conditions in the case under investigation resulted in many different paths but did not in further gains as far as fuel oil consumption is concerned.

Table 4. Fuel oil consumption (FOC) for the optimal route found with a clean hull when investigating in other conditions.

No. Case	Optimal Path with Clean Hull (t)	FOC: Optimal Path with Optimisation for Each Case (t)	Increase %
1		347.5	-
2	436.2	435.3	0.20
3	528.9	528.2	0.14
4	504.1	504.0	0.01
5	630.8	630.5	0.04

6.6. Ignoring Current Effects

Next, whether sea currents affect the route selection and counteract hull and propeller fouling is examined. As already mentioned, currents have been considered by correcting the speed through water value when calculating calm water resistance. A new optimization is performed but, in this case, the currents' effect is ignored. In Figure 13, a comparison between the optimal path found previously and the newly derived optimal path found without considering sea currents is presented, where both cases refer to the clean hull condition. When currents are considered, fuel oil consumption per nautical mile is significantly affected, as shown by intensive fluctuations (Figure 13). Moreover, fuel oil consumption is estimated to be about 345.8 t when considering currents, while 355.3 t is estimated when currents are ignored. The two different optimal paths are shown in Figure 14.

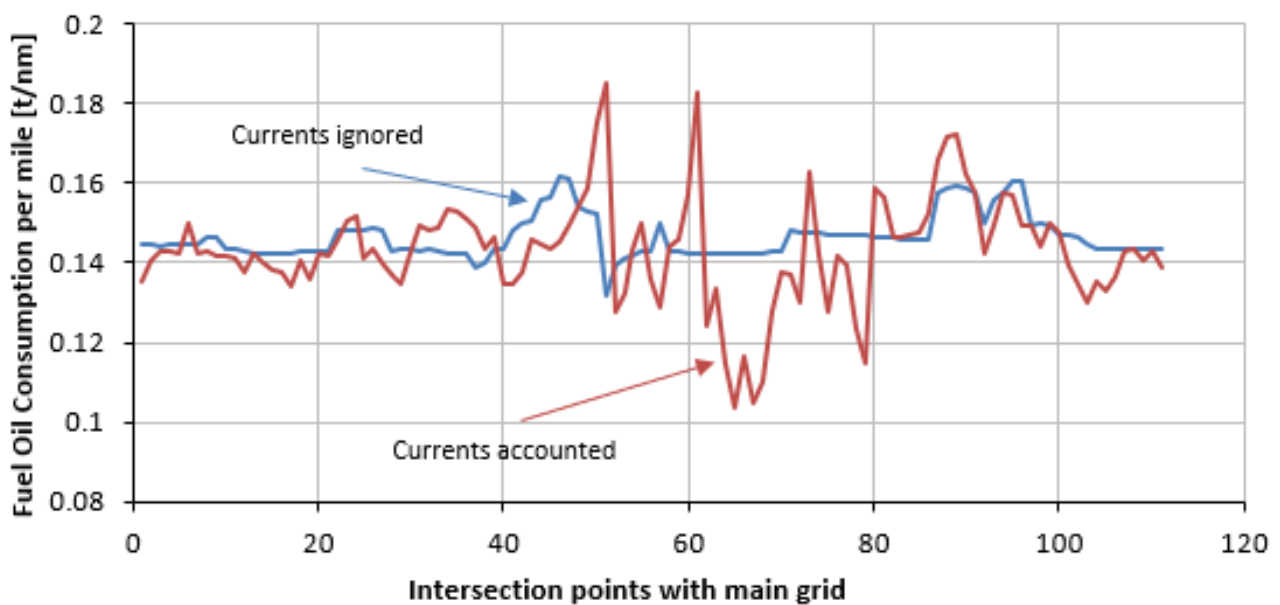


Figure 13. Fuel oil consumption per nautical mile for optimal paths found with and without the currents' effect for clean hull conditions.

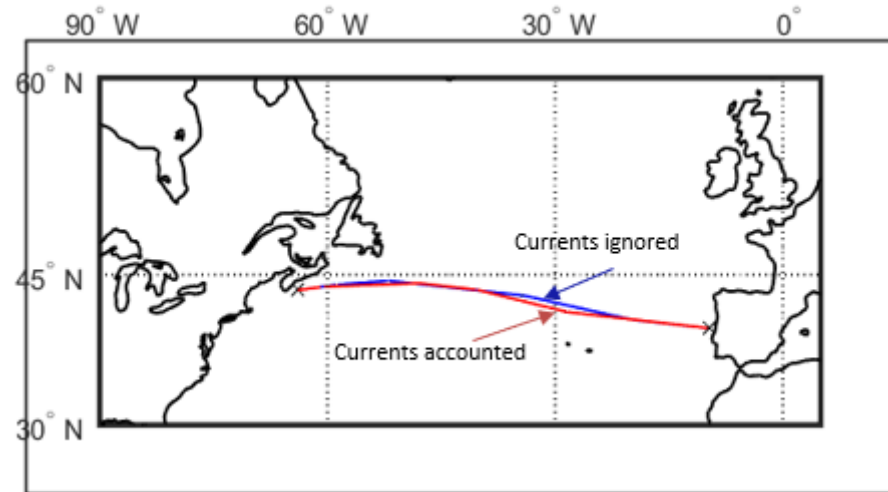


Figure 14. Optimal paths with (red route) and without (blue path) the currents' effect.

The fluctuations shown in Figure 13 are more noticeable when the hull is fouled and specifically when the heavy fouling condition is considered (Figure 15). This occurs because the optimization algorithm seeks favorable current paths (Figure 16) in order to decrease calm water resistance, which is extremely high and finally finds a path that requires 528.2 t of fuel instead of 540.6 t when currents are ignored. In Figure 17, the added wave resistance along the estimated optimal routes with and without the currents' effect under heavy fouling conditions is shown. When currents are ignored and speed remains constant, the major component for the minimization of fuel oil consumption and consequently for the minimization of the total resistance is the added wave resistance. This means that the algorithm seeks the optimal solution while trying to find a path where the significant wave height is low and/or where following seas are dominant. The two optimal paths for heavy fouling conditions with and without currents are shown in Figure 18.

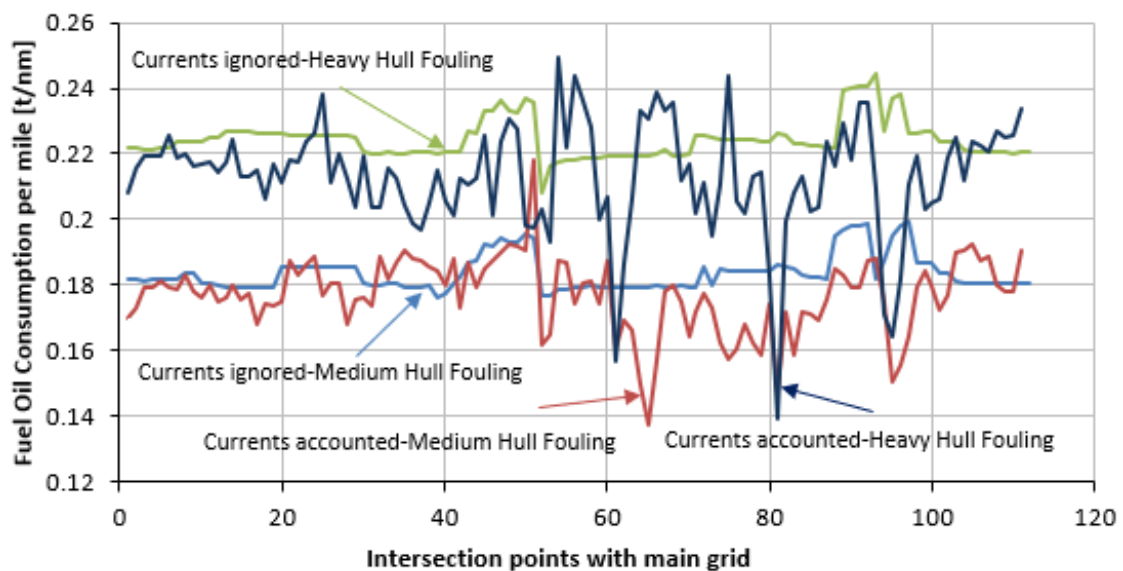


Figure 15. Fuel oil consumption per nautical mile for optimal paths with and without current effects under medium and heavy hull fouling conditions.

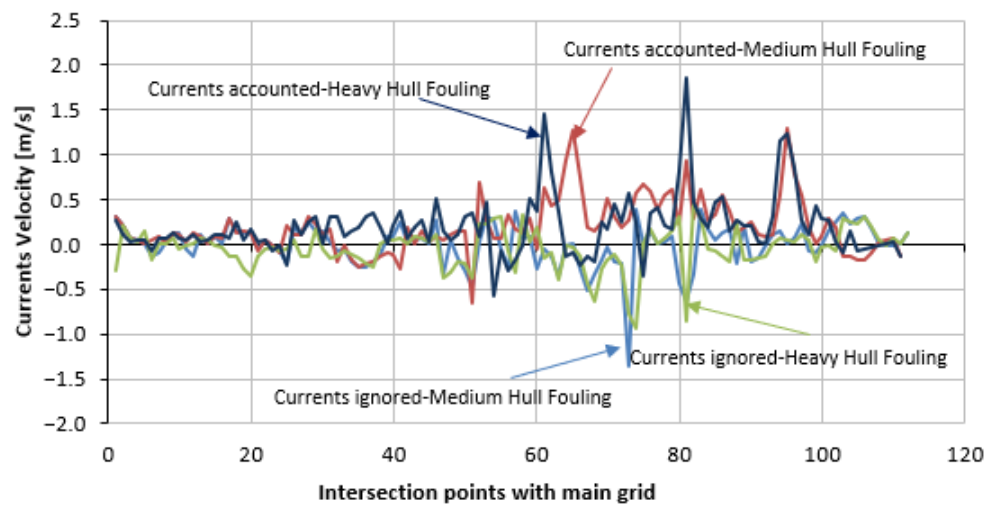


Figure 16. Prevailing current velocity along the optimal routes found with and without the currents' effects under medium and heavy hull fouling conditions.

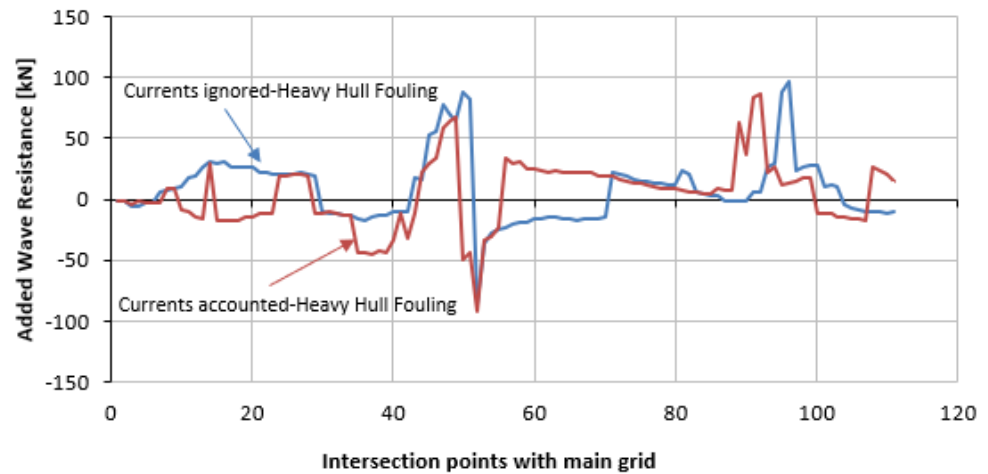


Figure 17. Added wave resistance along the optimal paths found with and without the currents' effect under heavy hull fouling conditions.

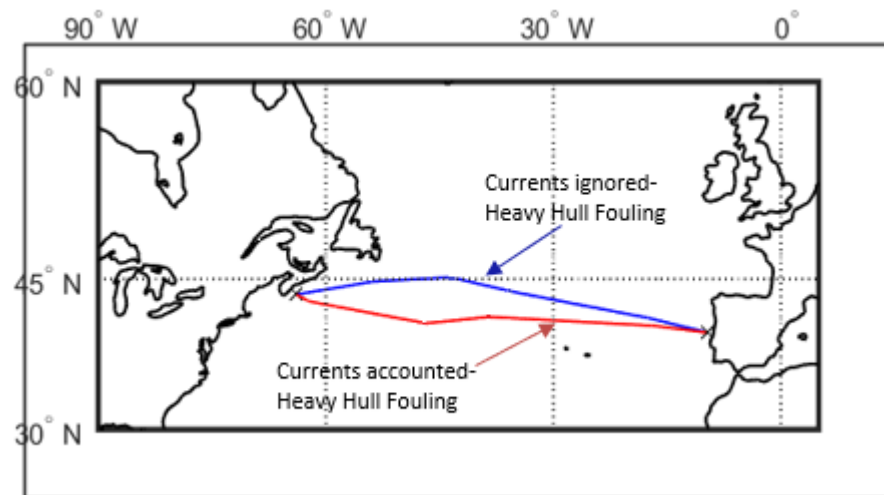


Figure 18. Optimal paths with (red route) and without (blue path) the currents' effect under heavy hull fouling conditions.

Next, a scenario where the optimized route without considering the currents' effect (path with blue color in Figure 18) is assumed to be the planned voyage path. However, in realistic conditions where sea currents are present, the fuel oil consumption would be equal to 546.9 t instead of 540.6 t, which was calculated without considering sea currents. In other words, ignoring the sea currents during the optimization process could result in an ostensible optimized route that leads to higher fuel oil consumption. For the case mentioned here, this misleading optimization can result in 1.16% more fuel oil consumption than the expected quantity and 3.55% more fuel oil consumption than the optimal consumption when sea currents were considered (path in red color in Figure 18). Table 5 summarizes the calculated fuel oil consumptions, voyage durations, and distances covered for the various scenarios examined. It shall be reminded that the so-called ostensible optimal route refers to the optimal path derived when currents were ignored from the optimization process; however, the calculation of fuel consumption that appears in Table 5 entails the sea currents' effect.

Table 5. Paths for heavy hull fouling conditions (Case 3).

	Orthodrome with/without Currents' Effect	Loxodrome with/without Currents' Effect	Optimal with/without Currents' Effect	Ostensible Optimal Route
FOC (t)	548.7/549.7	544.6/550.1	528.2/540.6	546.9
Voyage duration (h)	133.5	136.1	137/133.9	133.9
Distance (nm)	2402.2	2449.1	2477.9/2410.8	2410.8
FOC/distance (t/nm)	0.23	0.222/0.224	0.213/0.224	0.226

7. Conclusions and Future Work

In this study, a route planning tool is presented, emphasizing fouling and ocean currents' impact on optimal route selections. The operational deterioration due to the hull and propeller's fouling is highlighted, and the impact on fuel oil consumption is shown. Optimal route planning in conjunction with the fouling status of the hull and the propeller was systematically examined by considering the combined effect of hull and propeller fouling with respect to sea currents.

The optimization with different levels of fouling resulted in different identified paths, but no remarkable fuel oil consumption gains were obtained compared with the ones obtained when using the optimized path of the clean hull. Still, in other future cases, investigating further optimizations for fouled conditions is recommended, as is already performed in this study, because the optimal path with a clean hull may be unfeasible when fouling is considered.

Fouling affects frictional resistance, which is a major component of the calm water resistance of a vessel. Ocean currents also affect the calm water resistance of ships either positively or negatively. When fouling increases, the route planning process favors paths with a positive effect from sea currents and specifically to a greater extent than when the fouling level is low. If ocean currents are neglected in the route planning process, the predicted fuel oil consumption would differ from the actual one, and the estimated optimal routes may be unfeasible in real sea conditions for a demanded speed. This can lead to much higher fuel oil consumption than expected or to voluntary speed loss, both cause conflicts between ship owners and charterers. Route planning processes should take into consideration the level of the hull and/or propeller's fouling since not only fuel oil consumption would increase but also the path itself may change.

Apart from fouling and prevailing weather conditions, the fuel oil consumption and energy efficiency of a ship are also highly dependent on the ship's motion control system. Course keeping, efficient steering gear system, and rudder control can result in significant energy savings, a fact that should be investigated in future research.

Author Contributions: Conceptualization, N.T.; methodology, A.K. and N.T.; software, A.K.; formal analysis, A.K. and N.T.; data curation, A.K.; writing—original draft preparation, A.K. and N.T.; writing—review and editing, N.T.; visualization, A.K.; supervision, N.T. All authors have read and agreed to the published version of the manuscript.

Funding: This research received no external funding.

Institutional Review Board Statement: Not applicable.

Informed Consent Statement: Not applicable.

Data Availability Statement: Data sharing not applicable.

Conflicts of Interest: The authors declare no conflict of interest.

References

1. IMO. *Initial IMO Strategy on Reduction of GHG Emissions from Ships*; Resolution MEPC.304 (72); International Maritime Organisation: London, UK, 2018.
2. Bouman, E.A.; Lindstad, E.; Riialand, A.I.; Stromman, A.H. State-of-the-art technologies, measures and potential reducing GHG emissions from shipping—A review. *Transp. Res. Part D* **2017**, *52*, 408–421. [[CrossRef](#)]
3. Tadros, M.; Vettor, R.; Ventura, M.; Soares, C.G. Assessment of ship fuel consumption for different hull roughness in realistic weather conditions. *J. Mar. Sci. Eng.* **2022**, *10*, 1891. [[CrossRef](#)]
4. Liu, S.; Papanikolaou, A.; Bezunartea, B.A.; Baoguo, S.; Sreedharan, M. On the effect of biofouling on the minimum propulsion power of ships for safe navigation in realistic conditions. *J. Bioadhesion Biofilm Res.* **2021**, *37*, 194–205. [[CrossRef](#)]
5. IMO. *Interim Guidelines for Determining Minimum Propulsion Power to Maintain the Maneuverability in Adverse Conditions*; Resolution MEPC.232 (65); International Maritime Organisation: London, UK, 2013.
6. Schultz, M.P. Effects of coating roughness and biofouling on ship resistance and powering. *Biofouling J. Bioadhesion Biofilm Res.* **2007**, *23*, 331–341. [[CrossRef](#)] [[PubMed](#)]
7. Prpic-Orsic, J.; Vettor, R.; Faltinsen, O.M. The influence of route choice and operating conditions on fuel consumption and CO₂ emission of ships. *J. Mar. Sci. Technol.* **2016**, *21*, 434–457. [[CrossRef](#)]
8. Kytariolou, A.; Themelis, N. Ship routing optimisation based on forecasted weather data and considering safety criteria. *J. Navig.* **2023**, 1–22. [[CrossRef](#)]
9. Fang, M.C.; Lin, Y.H. The optimization of ship weather-routing algorithm based on the composite influence of multi-dynamic elements (II): Optimized routings. *Appl. Ocean. Res.* **2015**, *50*, 130–140. [[CrossRef](#)]
10. Kurosawa, K.; Uchiyama, Y.; Kosako, T. Development of a numerical marine weather routing system for coastal and marginal seas using regional oceanic and atmospheric simulations. *Ocean. Eng.* **2020**, *195*, 106706. [[CrossRef](#)]
11. Shin, Y.W.; Abebe, M.; Noh, Y.; Lee, S.; Lee, I.; Kim, D.; Bae, J.; Kim, K.C. Near-optimal weather routing by using improved A* algorithm. *Appl. Sci.* **2020**, *10*, 6010. [[CrossRef](#)]
12. Vettor, R.; Soares, C.G. Development of a ship weather routing system. *Ocean. Eng.* **2016**, *123*, 1–14. [[CrossRef](#)]
13. Chang, Y.C.; Tseng, R.S.; Chen, G.Y.; Chu, P.C.; Shen, Y.T. Ship routing utilizing strong ocean currents. *J. Navig.* **2013**, *66*, 825–835. [[CrossRef](#)]
14. Chen, C.; Sasa, K. Effect of ocean currents on ship navigation in the east China sea. *Ocean. Eng.* **2015**, *104*, 283–293. [[CrossRef](#)]
15. Yang, L.; Chen, G.; Zhao, J.; Rytter, N.G.M. Ship speed optimization considering ocean currents to enhance environmental sustainability in maritime shipping. *Sustainability* **2020**, *12*, 3649. [[CrossRef](#)]
16. Mannarini, G.; Coppini, G.; Lecci, R.; Turissi, G. Sea currents and waves for optimal route planning with VISIR. In Proceedings of the 16th International Conference on Computer and IT Applications in the Maritime Industries, Technische Universität Hamburg-Harburg, Hamburg, Germany, 15–17 May 2017.
17. Li, G.; Zhang, X. Green energy-saving robust control for ship course-keeping system based on nonlinear switching feedback. *Ocean. Eng.* **2023**, *268*, 113462. [[CrossRef](#)]
18. Zhang, G.; Chang, T.; Wang, W.; Zhang, W. Hybrid threshold event-triggered control for sail-assisted USV via the nonlinear modified LVS guidance. *Ocean. Eng.* **2023**, *276*, 114160. [[CrossRef](#)]
19. Zhang, G.; Wang, L.; Li, J.; Zhang, W. Improved LVS guidance and path-following control for unmanned sailboat robot with the minimum triggered setting. *Ocean. Eng.* **2023**, *272*, 113860. [[CrossRef](#)]
20. Zhang, C.; Wang, C.; Wei, Y.; Wang, J. Robust trajectory tracking control for underactuated autonomous surface vessels with uncertainty dynamics and unavailable velocities. *Ocean. Eng.* **2020**, *218*, 108099. [[CrossRef](#)]
21. Qin, J.; Du, J. Minimum-learning-parameter-based adaptive finite-time trajectory tracking event-triggered control for underactuated surface vessels with parametric uncertainties. *Ocean. Eng.* **2023**, *271*, 113634. [[CrossRef](#)]
22. Holtrop, J.; Mennen, G.G.J. An approximate power prediction method. *Int. Shipbuild. Prog.* **1982**, *29*, 166–170. [[CrossRef](#)]
23. Liu, S.; Papanikolaou, A.; Zaraphonitis, G. Prediction of added resistance of ships in waves. *Ocean. Eng.* **2011**, *38*, 641–650. [[CrossRef](#)]

24. Liu, S.; Papanikolaou, A.; Zaraphonitis, G. Practical approach to the added resistance of a ship in short waves. In Proceedings of the Twenty-Fifth (2015) International Ocean and Polar Engineering Conference, Kona, Big Island, HI, USA, 21–26 June 2015.
25. Blendermann, W. Parameter identification of wind loads on ships. *J. Wind. Eng. Ind. Aerodyn.* **1994**, *51*, 339–351. [[CrossRef](#)]
26. ITTC. ITTC Recommended procedures and guidelines: Preparation, conduct and analysis of speed/power trials. In Proceedings of the International Towing Tank Conference, Wuxi, China, 17–22 September 2017.
27. MATLAB. *Global Optimisation Toolbox User's Guide*; The MathWorks, Inc.: Natick, MA, USA, 2022.

Disclaimer/Publisher's Note: The statements, opinions and data contained in all publications are solely those of the individual author(s) and contributor(s) and not of MDPI and/or the editor(s). MDPI and/or the editor(s) disclaim responsibility for any injury to people or property resulting from any ideas, methods, instructions or products referred to in the content.